Article:
Myllykyla, E., Lavonen, T., Stennett, M. et al. (3 more authors) (2015) Solution composition and particle size effects on the dissolution and solubility of a ThO2 microstructural analogue for UO2 matrix of nuclear fuel. Radiochimica Acta, 103 (8). pp. 565-576. ISSN 0033-8230

https://doi.org/10.1515/ract-2014-2271

Solution composition and particle size effects on the dissolution and solubility of a ThO_2 microstructural analogue for UO_2 matrix of nuclear fuel

E.Myllykylä[1], T.Lavonen[1] , M. Stennett[2] , C.Corkhill[2], K.Ollila[1] , N. Hyatt[2]

[1]VTT Technical Research Centre of Finland, Espoo, Finland

[2]Immobilisation Science Laboratory, Department of Materials Science and Engineering, The Unversity of Sheffield, Mappin Street, Sheffield, S1 3JD,UK

Abstract

The objective of this study was to investigate the dissolution rate of ThO_2 which was synthesised to approximate, as closely as possible, the microstructure of UO_2 in a nuclear fuel matrix. The optimal sintering temperature for ThO_2 pellets was found to be 1750°C, which produced pellets with a microstructure similar to UO_2 nuclear fuel pellets, with randomly oriented grains ranging in size from 10 to 30 µm. Dissolution was conducted using ThO_2 particles of different size fractions (80 to 160 µm and 2 to 4 mm) in the presence and absence of carbonate in solutions with pH from 2 to 8. Dissolution rates were calculated from Th released from the solid phase to solution. Particles of ThO_2 were also leached with 1 M HNO_3 at 80 °C in order to investigate the morphological changes at the particle surfaces. The concentration of Th was found to be $\geq 10^{-9}$ mol/L at pH ≤ 4, lower than the theoretical solubility of crystalline ThO_2. At higher pH values, from 4 to 8, the measured concentrations (10^{-10} to 10^{-12} mol/L) were between the theoretical solubility of ThO_2 and $Th(OH)_4$. Grain boundaries were shown to exert an influence on the dissolution of ThO_2 particles. Using high resolution aqueous solution analysis, these data presented here extend the current understanding of Th solubility in solution.

1. Introduction

Thorium dioxide (ThO_2) is isostructural to UO_2, sharing the same fluorite-type structure (space group Fm3m), making it a useful structural analogue for spent nuclear fuel, which is predominantly composed of UO_2 (>95%). However, unlike $U^{(IV)}O_2$, $Th^{(IV)}O_2$ is not redox active since Th has only one prevailing oxidation state, +4 [1]. The next generation applications of nuclear energy have shown interest towards

thorium [2]. As a fuel, thorium has many beneficial properties, such as high fusion temperature, good sintering capability, resistance against radiation damage, greater abundance in the Earth's crust compared to U, and the possibility for transmutation [2].

The preferred option worldwide for the long-term disposal of spent nuclear fuel, and potentially future Th-based nuclear fuels, is disposal in a deep geological disposal facility, several hundreds of metres below ground [3-4]. In this environment, the release of Th and other radionuclides to the geo- and bio-spheres will be controlled by the dissolution of the fuel by groundwater. Hence it is necessary to understand the dissolution behaviour of the fuel and the solubility of radionuclides in groundwater.

In the literature, the solubility values for ThO_2, and also the hydrolysis constants of thorium, show great discrepancies e.g. Vandenborre et al. 2008, 2010 Neck and Kim, 2001 [5-7]. The main reasons for these differences include: the tendency of Th to undergo polynucleation and colloid formation, its strong absorption to surfaces, and the low solubility of Th^{4+} hydroxide and hydrous oxide. The presence of complexing ligands like CO_3^{2-} [8] has also been shown to increase the solubility of ThO_2. These characteristics of thorium together with the relatively low solubility of ThO_2(cr) make solubility studies of ThO_2 challenging.

The solubility product values have been observed to vary between ThO_2 (microcryst.) ($\log K°sp = -53 \pm 0.5$) and $Th(OH)_4$ (am) ($\log K°sp = -46.7 \pm 0.9$) [9-11] depending on the crystallinity and crystallite size of the Th(IV) oxide and hydroxide or oxyhydroxide phase. The predicted value, according to the Equation of Schindler [12] and experimental data, for ThO_2 (cr) is $\log K°sp = -54.2 \pm 1.1$ [9]. In addition to crystallinity, surface phenomena have been mentioned as a possible factor affecting the solubility properties. Vanderborre et al. 2010 [6] combined investigation of solid surfaces with leaching experiments, and isotopic exchange methods to understand the discrepancy in solubility values and to describe the reversibility in the exchange mechanism. They observed that the dissolution mainly occurred at grain boundaries and showed variation between different sites, indicating "local solubility" effects. In addition, the usage of ^{229}Th spiking revealed dynamic dissolution/precipitation reactions on the solid/solution interface.

Many solubility studies have been conducted with amorphous phases of ThO_2 [13-17]. The higher solubility of amorphous-phase ThO_2, compared to well-crystalline ThO_2, simplifies the analysis of Th in liquid phase, because the amorphous phases have higher solubility. Crystalline phases of ThO_2 have also been studied [18-19]. Hubert et al. [18] observed the effect of surface properties on the leachibility of solid ThO_2. Factors including specific surface area, surface state and size of aggregates were found to have influence on the apparent solubility. However, when the leaching rate was normalized to surface area, it seemed to be independent of the surface charazteristics.

The aims of this study were to prepare crystalline ThO_2 pellets having a microstucture similar to that of spent UO_2 nuclear fuel pellets and to conduct dissolution experiments, in order to further evalauate the relative solubility of ThO_2 phases. We report the initial release rate of Th during the first 20 to 40 days of dissolution. Solubility studies were extended to 100 to 120 days to gain a thorough understanding of the solubility limit of different ThO_2 phases.

The first experiment series in the solubility and dissolution rate studies was conducted with 2 to 4 mm particles in 0.1 M NaCl and 0.01 M NaCl (with 2 mM $NaHCO_3$) solutions under atmospheric conditions. The second experiment series was conducted with two particle sizes, 60 to 180 μm and 2 to 4 mm, in 0.1 M NaCl and 0.01 M HNO_3 solutions in an Ar glove box to exclude atmospheric carbon. In addition, several leaching experiments were run in 1 M HNO_3 solution and at 80 $^{\circ}$C in order to observe surface changes during dissolution in a relatively short time scale.

2. Experimental

2.1 Preparation of ThO_2 pellets

Thorium dioxide pellets were prepared to approximate the microstructure of UO_2 fuel and CeO_2 analogues for UO_2 [19-21], with grain sizes in the range of 5 – 30 μm, with randomgrystallographic orientation. The precursor material was ThO_2 powder (BDH (British Drug House) Laboratory Reagents Ltd., Lot No: G83757/541012), which was confirmed as pure ThO_2 by powder X-ray Diffraction using STOE Cu-IP diffractometer, with a Cu kα source (diffraction patterns were collected at $5 < 2\theta < 60°$ at 2° min^{-1}, using a step size of 0.02°). 1g of ThO_2 powder was placed within a 10 mm diameter hardened stainless steel die and uniaxially pressed with a load of 100 MPa. The green density (i.e. compacted density) of the pressed compacts was calculated prior to sintering by measuring the pellet mass and geometry. Green ThO_2 pellets, placed on stabilised zirconia setter plates, were sintered in triplicate for 4 hours at temperatures between 1300 and 1750 °C in a standard air atmosphere muffle furnace. Pellets were heated and cooled with a ramp rate of 5 °C min^{-1} and held at the sintering temperature for 4 hours.

The sintered density of the pellets was measured using geometric and water immersion (Archimedes) methods. All density measurements were performed in triplicate.

For surface analysis only (i.e. not dissolution experiments) ThO_2 pellet samples were polished to a 1μm finish using SiC paper and diamond paste. A final mechanico-chemical etch was performed using a 0.06 μm colloidal silica solution. In order to develop a grain boundary texture at the surface of the pellets, annealing was performed at 90 % of the sintering temperature, at a ramp rate of 5°C min^{-1} and held at the annealing temperature for 1 hour. Pellets were imaged using an optical microscope. Analysis of the crys-

tallographic orientation and grain size distribution of pellets was performed using Electron Backscatter Diffraction Analysis (EBSD) (Oxford Instruments) in conjunction with a Sirion Field Emission SEM. EBSD maps of 100 μm^2 were obtained at an accelerating voltage of 20 kV and a 0.5 µm step size. Grain orientation analysis was performed on > 10000 grains, using HK Channel 5 software (Oxford Instruments).

2.2 Fragmentation of the pellets

For the experiments, the ThO_2 pellets were crushed using a percussion mortar. Particles between 2 and 4 mm were selected with tweezers and washed four times in isopropanol followed by gravitational settling in an attempt to remove adhering fine fragments. This was not successful, so the particles were soaked one at a time on isopropanol followed by ethanol and then dried in a desiccators.

The intact pellets of ThO_2 (~ 20 g) were fragmented to smaller particle sizes. In order to avoid contamination by the milling media, the electrodynamic fragmentation method [22-23] was selected to comminute the pellets into the required particle sizes. The principles of the method can be briefly described, as follows: Electrical energy in the form of repeated high voltage pulses is applied to the samples immersed in a dielectric process liquid. Dielectric liquids, like water, have a high dielectric strength, when the voltage rise time is kept below 500 ns. As such, the discharges are forced to occur through the immersed material. Plasma channels and explosions were generated inside the pellets and the resulting shockwaves produced fracturing and physical breakdown.

Fragmentation was conducted using a batch scale selFrag instrument available at the Research Laboratory of the Geological Survey of Finland.

The commercialized 1.7 tons instrument designed for the c.a. 1 kg sample was used. Approximately 20 grams of ThO_2 pellets were subjected to a two stage treatment. The process liquid used was regular tap water. After the first fragmentation the sample was classified using 0.2 mm net sieve, and the remaining oversized fraction (ca. 14 g) was re-fragmented. The process parameters used for both the first and second fragmentation procedure were: number of pulses 400, e-gap 10mm, freq. 3 and voltage 120-140 kV.

The fragmented material was washed using tap water and any iron contamination from the electrode was removed using hand magnets. The final product for use in dissolution experiments was sieved to a particle size fraction of 80 to 160 µm.

2.3 Dissolution experiments

The first experiment series of solubility and dissolution rate studies were conducted with 2 to 4 mm particles in 0.1 M NaCl and 0.01 M NaCl (with 2 mM $NaHCO_3$) solutions under atmospheric conditions (solutions were prepared

from suprapure (99.99%, Merck) NaCl and $NaHCO_3$ (ACS,Reag.Ph Eur, Merck KGaA) in MilliQ-water). Experiments were conducted in triplicate at room temperature (23 ± 1 °C) for up to 115 days. Approximately 300 mg of crushed ThO_2 particles were placed in a 60 ml high density polypropylene vessel with 50 ml of leaching solution. The second experiment series was conducted with two particle sizes (60 to 180 μm and 2 to 4 mm), both in 0.1 M NaCl and 0.01 M HNO_3 (prepared from concentrated HNO_3, ULTREX II by J.T Baker) within an Ar glove box at 25 ± 1 °C. The duration of these experiments, conducted in duplicate, was 93 days. Approximately 150 mg of particles were placed in a 60 ml vessel with 50 ml of leaching solution. Polypropylene vessels were used for experiments with 0.01M HNO_3, and high density perfluoroalkoxy Teflon vessels were used for 0.01M NaCl solutions, in order to decrease the potential sorption of Th to the reaction vessel under near neutral conditions.

In the first experiment series, conducted under atmospheric conditions, sampling was performed at 0, 1, 3, 6, 15, 24, 31 41, 48, 79, 100 and 115 days by withdrawing a 2.5 ml sample. Each sample was ultrafiltered with a Pall Mall filtration device with 10 kD (~1 nm) molecular cut off, using centrifugation (6000 rpm, 1 h). In addition, some samples were taken and not filtered. The pH was measured directly from the test solution with ROSS combination electrode at the beginning of the experiment and after 35 days of reaction time.

Sampling of the experiment series under an Ar atmosphere was conducted at 0, 1, 2, 5, 7, 9, 14, 21, 30, 43, 57, 70 and 89 days. Both non-filtered and ultrafiltered samples (as above) of 2.5 ml were taken. The pH was measured in solutions under Ar glovebox conditions using a ROSS combination electrode, directly from the reaction vessel within every second sampling.

The concentration of ^{232}Th in non-filtered and ultrafiltered samples was analysed with a High Resolution sector Field Inductively Coupled Plasma-Mass Spectrometer (HR-ICP-MS, Element2 by ThermoScientific). Standard solutions with known concentrations were diluted from AccuTrace™ Reference Standard SQS-01. A control sample for analysis was prepared from standard CLMS-1 solution by SPEX. All the blank, standard and control samples contained a known amount of an internal standard, indium. Analyses of ^{232}Th were performed with HR-ICP-MS in low resolution mode (R≈ 300). The detection limit for thorium was calculated as six times the standard deviation of the ion counts obtained for the sample blanks (ten replicates) , divided by the sensitivity of the 1 µg/L standard solution of Th. The detection limit for thorium was therefore found to be between $1 \cdot 10^{-12}$ mol/L and $4 \cdot 10^{-12}$ mol/L depending on the solution matrix and daily efficiency of the instrument. The uncertainty of the Th analyses increased up to 10 % when the measured concentration was close to the detection limit. With higher concentration the uncertainty of the analysis was a few percent.

The dissolution rate ($r_{^{232}Th}$ [molg^{-1}s^{-1}]) for ThO_2 was calculated by using equation (1)

$$r_{^{232}Th} = \frac{V}{m}\frac{dc_{^{232}Th}}{dt} \quad (1)$$

where V is the volume of the solution [L], m is the mass [g] of ThO_2 and dc/dt is the slope (linear fit) determined from the evolution of ^{232}Th release as function of time [molL^{-1}s^{1}]. This analysis is similar to that applied to consideration of mineral dissolution elsewhere e.g. in Rozalen et al, 2008, Malmström M., 1996, Brady and Walther 1990 [24-26].

The surface area was calculated by assuming that the ThO_2 particles are cubes (which is not true as is commonly known see e.g. [27]) and using the measured density of ThO_2 approximately 9 g/cm^3 (~93 % of the theoretical 9.86 g/cm^3) [28].

$$\rho_{ThO_2} = \frac{m_{ThO_2}}{V_{tot,ThO_2}}$$

$$V_{grain} = d^3$$

$$N_{grain,ThO_2} = \frac{V_{tot,ThO_2}}{V_{grain}}$$

$$A_{grain,ThO_2} = 6d^2_{grain,ThO_2}$$

$$SA_{tot,ThO_2} = N_{grain,ThO_2}A_{grain,ThO_2} = 6\frac{m_{ThO_2}}{\rho_{ThO_2}}\frac{1}{d_{ThO_2}} \quad (2)$$

2.4 Characterization of leached ThO_2 surfaces with SEM

The ThO_2 particles were subjected to leaching experiments in acidic conditions and at elevated temperatures in order to monitor the evolution of surface morphology during dissolution. For detailed characterisation of the pellet morphology during dissolution, see Corkhill et al. [29]. Surface characterisation was performed on particles in the 80 to 160 µm size fraction, following particles were used for surface characterization after immersion in a 1 M HNO_3 (~ pH 1) solution at 80 °C for 2 and 4 weeks under Ar atmosphere. Prior to heating the reaction vessels were placed in a sealed steel container under Ar atmosphere of the glove box to maintain argon atmosphere. . Surfaces of ThO_2 subject to this treatment were studied with SEM (JEOL JSM-900LV with Oxford Instruments) using an accelerating voltage of 20 kV and beam size of 10 µm.

3. Results and Discussion

3.1 The properties of sintered ThO_2 pellets

Figure 1 shows the X-ray diffraction analysis of ThO_2 power, confirming the purity of the starting material. The characteristics for a suitable UO_2 fuel analogue include a grain

size on the order of 8 – 15 μm, a sintered density of > 95.5 % theoretical density, and randomly orientated grains. The sintering temperature was varied in order to determine the optimal sintering conditions to create such characteristics. Figure 2 shows the densities of the sintered pellets as a function of sintering temperature.

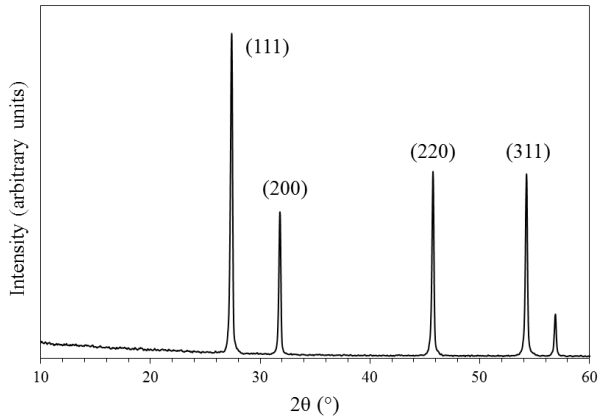

Fig. 1. XRD pattern for thorium dioxide powder used to synthesise UO_2-fuel analogue pellets for dissolution experiments.

The density of the pellets increased with increasing sintering temperature up to 1750 °C (Fig. 2); this temperature gave a density of 93 % of the theoretical density, which is slightly below optimal for a UO_2 analogue. Heating at higher temperatures caused a loss of pellet integrity, therefore 1750°C was the highest sintering temperature evaluated. The increase in density with increasing sintering temperature is consistent with decreasing porosity and increasing grain size, as shown by optical microscope images in Figure 3. The grain size was found to increase from 2 – 10 μm at 1650 °C to 10 – 30 μm at 1750°C (Table 1). Sintering at 1750 °C was, therefore, found to give the optimum grain size and density achievable. EBSD analysis was performed to determine grain size and crystallographic orientation. The average grain size was found to be 13 μm (based upon analysis of >10000 grains). Figure 4 shows that synthesis at 1750°C produced grains that were randomly orientated in the {111}, {100} and {101} crystal planes
.

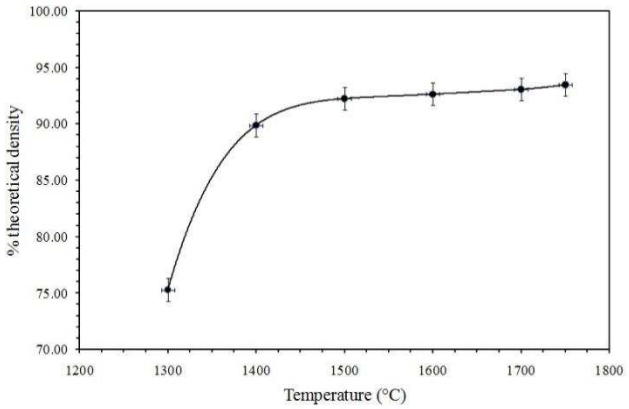

Fig. 2. Density of the sintered ThO_2 as function of sintering temperature.

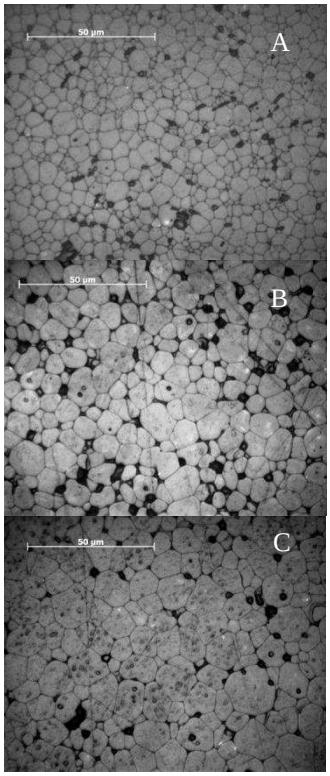

Fig. 3. Optical microscopy images of the ThO_2 pellet surface sintered at 1600 (A), 1700 (B), and 1750 °C (C).

Table 1. The grain size of ThO_2 pellets as a function of sintering temperature.

Sintering temperature (°C)	Grain size (µm)
1600	2-10
1700	5-20
1750	10-30

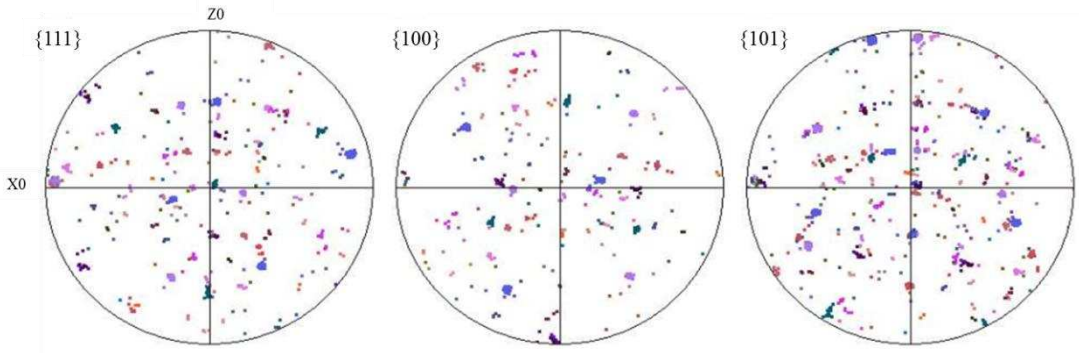

Fig. 4. Representative crystal orientations of a pressed pellet of ThO_2 sintered at 1750 °C and annealed at 1500 °C to develop grain structure. Pole figures show the random orientation of the grains in the {111}, {100} and {101} crystal planes.

3.2 Particle characteristics after selFrag HV pulsing

Fragmentation of the ThO_2 pellets produced randomly shaped ThO_2 particles, as confirmed by optical and electron microscopy (Figs. 5 and 6). Similar randomly broken grains

typically result from applying conventional comminution techniques e.g. grinding. However, adhered fines, normally seen in SEM images showing products from conventional comminution, were not observed, due to the pulse fragmentation procedure. Adhere-particle free surfaces can be regarded as ideal samples for the dissolution experiments undertaken in this study.

The particles exhibited two main textures: those with a grain boundary texture and those without, as shown in Figure 6. Grain boundaries were formed in these particles through two processes. Firstly, prior to fragmentation, surfaces of the original pellets developed a grain boundary texture through high temperature annealing. It may also be possible that such surfaces originate from the pulse fragmentation process, which forces liquid through grain boundaries to break the particles apart, leaving behind several surfaces with a grain boundary texture.

Fig. 5. An image of 80 to160 µm ThO_2 particles taken with a biocular stereomicroscope.

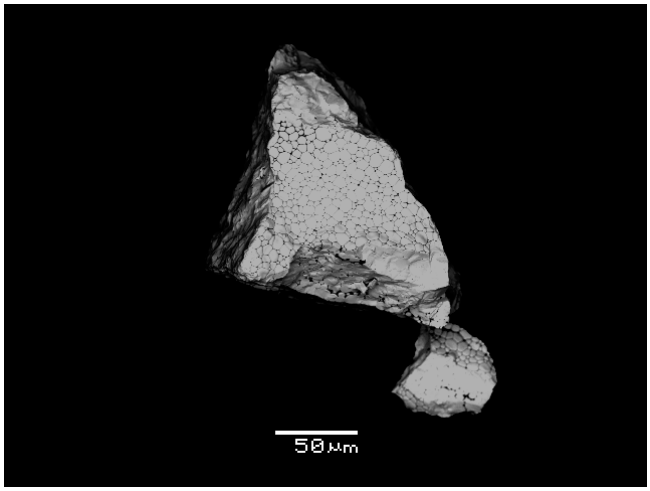

Fig. 6. SEM image of 80 to160 µm ThO_2 particle crushed using the SelFag pulse fragmentation technique (330 x magnification).

3.3 Dissolution experiments

3.3.1 ThO_2 dissolution under atmospheric conditions

Figure 7 shows the dissolution data for ThO_2 particles (2 - 4 mm) leached in air in 0.1 M NaCl or in 0.01M NaCl with 2 mM $NaHCO_3$. In the solution containing carbonate (Fig. 7a), a maximum concentration of Th of ~10^{-10} mol/L was measured in non-filtered samples after 6 days of dissolution. After 40 days the concentration plateaued at approximately 10^{-12} mol/L. The ultrafiltered samples reached a concentration of between 10^{-11} and 10^{-12} mol/L at 40 days, preceded by a steady increase in concentration from 10^{-13} mol/L. The initial pH value of 8.4 decreased slightly to pH 8.2 during the first 35 days of the experiment. In the 0.1 M NaCl solution, shown in Figure 7b, the increase of the measured concentration was not obvious; the concentrations in both non-filtered and ultrafiltered samples are scattered (Fig 7b) most probably due the concentrations occurring close to the analytical detection limit ($1 \cdot 10^{-13}$ mol/L). The concentration of Th in the ultrafiltered samples decreased below this detection limit of after 48 days sampling. The initial pH of the 0.1 M NaCl increased from 5.4 to pH 5.8 during the first 35 days of the experiment.

When comparing the results of the two experiments, the solubility and the dissolution rates were greater in the solution containing carbonate, ($1 \cdot 10^{-13}$ mol dm^{-3} d^{-1}), likely due to,the formation of Th-containing carbonate/hydroxide complexes. In the absence of carbonate (0.1 M NaCl solution) there was no clear trend, however, if the dissolution rate is estimated from ultrafiltrated samples, the obtained value was found to be $2 \cdot 10^{-14}$ mol dm^{-3} d^{-1}, an order of magnitude less than that in the carbonate-containing solution. In the oxic conditions utilised in these experiments (which were conducted in air), dissolved carbon dioxide from the atmosphere may have had a slight solubility increasing effect in the bi-carbonate-free solution. The increasing effect of carbonate complexation on the solubility of thorium in each of the applied experimental conditions was previously evaluated by geochemical modelling (PHREEQC) [30]. A second set of experiments was therefore conducted under inert Ar atmosphere, to exclude such effects.

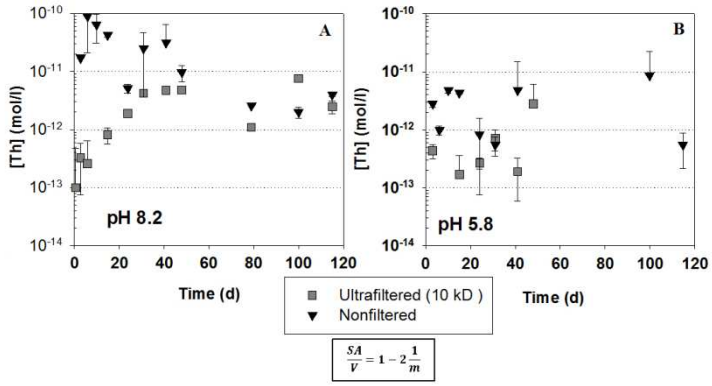

Fig. 7. Evolution of Th concentrations in ultrafiltered and non-filtered experiments of 2 – 4mm ThO_2 particle dissolution in (A) 0.01 M NaCl with 2 mM $NaHCO_3$ and (B) in 0.1 M NaCl, both under atmospheric conditions, at a temperature of 23°C.

3.3.2 ThO_2 dissolution in anaerobic conditions

The dissolution data resulting from the leaching of 80 to 160 µm and 2 – 4 mm particles of ThO_2 in 0.1 M NaCl under an Ar atmosphere are shown in Figure 8. Unfiltered samples arising from the smaller size fraction (80 to 160 µm) demonstrated a relatively rapid initial increase in Th concentration to ~$8 \cdot 10^{-10}$ mol/L after 2 days of dissolution, followed by a progressive decrease to $4 \cdot 10^{-11}$ mol/L by 89 days (Fig 8a). Under the same conditions, ultrafiltered samples (Fig. 8b) gave a maximum Th concentration of ~ $4 \cdot 10^{-10}$ mol/L after 7 days of leaching. After 9 days of dissolution, the concentration of Th decreased below $1 \cdot 10^{-11}$ mol/L and remained at ~ $2 \cdot 10^{-12}$ mol/L after 57 days.

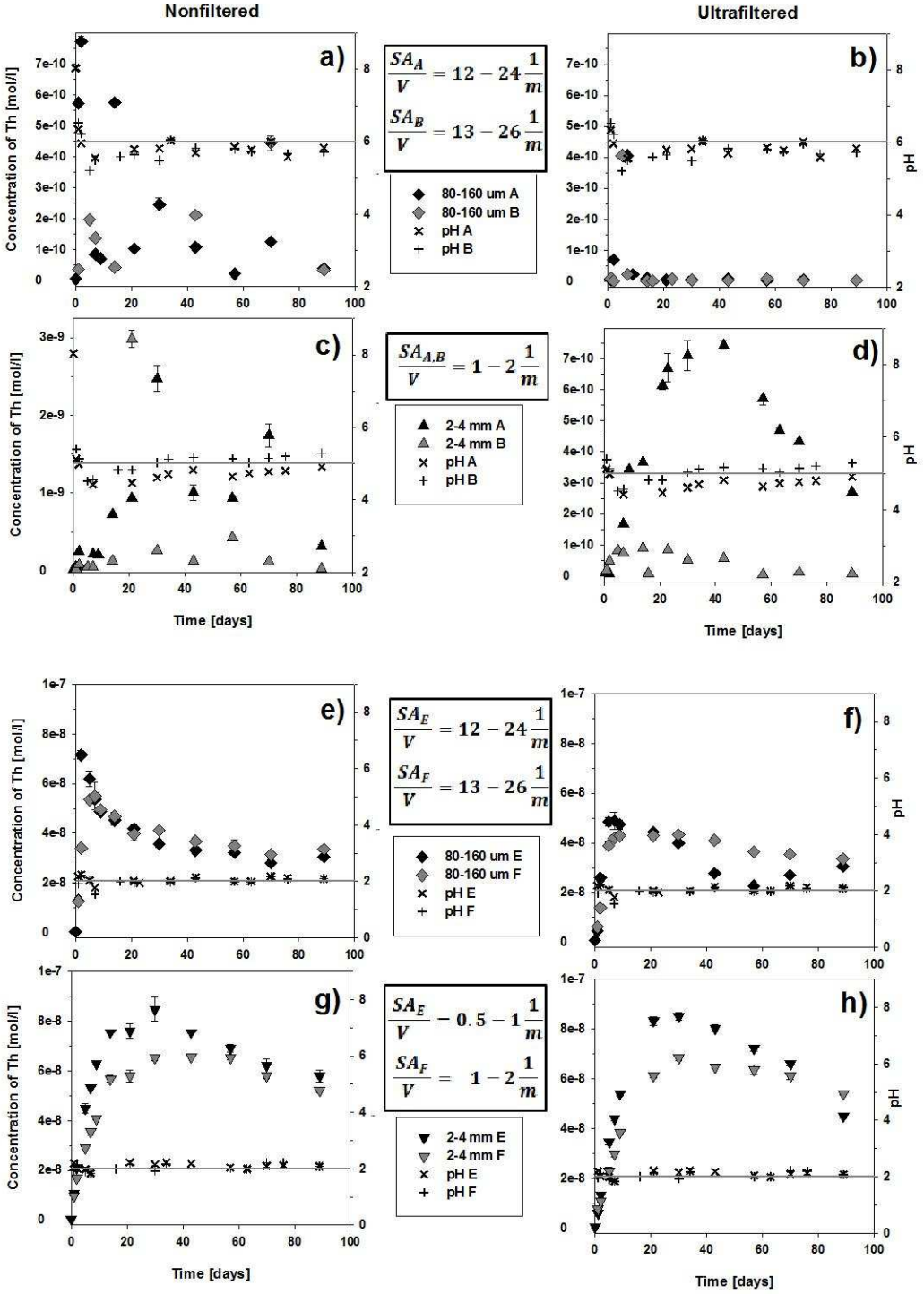

Fig. 8. The evolution of Th concentration and pH in 0.1 M NaCl (a, b, c, d) and in 0.01 M HNO_3 (e, f, g, h) with particle sizes 80 to 160 µm (a, b, e, f) and 2 to 4 mm (c, d, g, h) at 25 ℃. The results of the Non-filtered samples are given on the left and the ULTRA-filtered ones on the right. The solid lines were sketched to guide the eye to follow the pH values. Filtrations, solutions and particle sizes presented here are also shown with references to this Fig. in Table 2. (symbols A and B (E and F) in legend boxes refer to the parallel experiments).

The maximum concentrations of Th were reached after 23 days of dissolution ($3 \cdot 10^{-9}$ mol/L and $7.4 \cdot 10^{-10}$ mol/L for

non-filtered and ultrafiltered samples, respectively). This suggests that dissolution and precipitation / sorption kinetics are also slower in these samples, which is likely related to the lower surface area resulting from the larger particle size; the saturation limit is reached more slowly because there is less surface area available for sorption and precipitation of secondary Th compounds.

The initial pH of the 2- 4 mm ThO_2 dissolution experiments was found to decrease rapidly from pH 8 to between pH 5 and pH 6, where it remained for the duration of the experiment. This unexpected result is likely due to the leaching of H^+ from incompletely rinsed reaction vessels.

Parallel, ultrafiltered experiments conducted for the 2 – 4 mm particle size (designated A and B, Fig. 8d)showed considerable variation in concentration, by almost one order of magnitude. This may be due to the influence of pH in the test solutions; experiment A had a pH value of 4.8, while experiment B gave a pH value of 5.3. At the conclusion of the experiment, the Th concentrations were $7 \cdot 10^{-12}$ mol/L (experiment A, pH 4.8) and $3 \cdot 10^{-10}$ mol/L (experiment B, pH 5.3). While the difference in pH was only small, these observations confirm the fact that the solubility of ThO_2 is highly dependent on the H^+ activity in the solution [9-11].

3.3.3 ThO_2 dissolution as a function of particle size

To investigate further the influence of particle size on the dissolution of ThO_2, experiments were conducted in 0.01 M HNO_3, where dissolved Th concentrations far exceeded the analytical detection limit of Th, allowing for an accurate determination of the effects of particle size on dissolution rate.. For 80 to 160 µm particles of ThO_2 (Figs. 8e and f), the concentration in the non-filtered samples increased rapidly to $5 \cdot 10^{-8}$ mol/L after 5 days of dissolution. Similarly, in the ultrafiltered samples, the Th concentration increased to $4 \cdot 10^{-8}$ mol/L over the same time period. After this initial rapid dissolution, the concentration of Th decreased to levels between $3 \cdot 10^{-8}$ and $4 \cdot 10^{-8}$ mol/L for the duration of the 90 days experiment, in both non-filtered and ultrafiltered samples.

For the 2 to 4 mm ThO_2 particles, the initial dissolution rate was slower than that of the smaller particle size. The maximum concentration of Th was reached after 30 days of dissolution, giving values of $6.5 \cdot 10^{-8}$ mol/L and $8.5 \cdot 10^{-8}$ mol/L for duplicate samples (Fig. 8g -h). The final concentration of Th was ~5 x 10^{-8} mol/L after 90 days, which was slightly higher than the final concentration arising from the smaller particle size (~3 x 10^{-8} mol/L) (Figs. 8e-f).This suggests that particles with a greater surface area (e.g. 80 – 160 µm size fraction) reach lower maximum concentrations than particles with lower surface area (e.g. 2 – 4 mm particles) a result of more surface sites available for sorption of secondary precipitates. Such precipitates attenuate further dissolution of the surface. A similar effect was observed for particles subject to dissolution in 0.1 M NaCl (described above). However, unlike the dissolution experiments conducted in 0.1M NaCl, where dissolution rates were clearly affected by filtration and hence, the presence of colloidal

species, the evolution of Th concentration in 0.01M HNO_3 was independent of the sampling method; the concentrations of the ultrafiltered samples were very similar to the non-filtered ones. This indicates that secondary phases or colloids did not play a significant role in these experiments. One possible explanation may be effects arising from high energy sites on the surface, for example grain boundaries (shown in Fig. 6). The larger particles comprise surfaces with more grains than the smaller particles, therefore they have a greater number of grain boundaries. In a recent study [29] it was found that grain boundaries of ThO_2 and CeO_2 analogues for UO_2 fuel dissolved very rapidly in 0.01M HNO_3. Therefore, the higher maximum concentrations found for the large particles may be due to dissolution of grain boundaries

3.3.4 Dissolution rates of ThO_2

The initial dissolution rates of ThO_2 under the experimental conditions investigated were calculated from the evolution of Th concentration during the period of release of Th into solution, which took between 5 to 30 days, depending on the liquid phase in question.

Calculated rates were obtained from linear regression of these data, and are given in Table 2. The results clearly show the pH dependence of the dissolution rate and the increasing effects of carbonate concentration and particle size . The dissolution rates were found to be greatest at low pH and in the presence of carbonate. Small differences were also observed between parallel experiments and in the comparison between results calculated from non-filtered and ultrafiltered samplings.

The presence of carbonates is known to increase the solubility of ThO_2, which can have a significant effect on the behaviour of Th(IV) in natural groundwaters. One order of magnitude increase in $[CO_3^{2-}]$ has been shown to increase the solubility of hydrous ThO_2(am) by up to five orders of magnitude [31]. Two mononuclear carbonate complexes of Th(IV), $Th(OH)_3CO_3^-$ and $Th(CO_3)_5^{6-}$, have been reported [31, 32]. Considerably higher Th(IV) solubility in the Th(IV)-H_2O-CO_3^{2-} system, indicated the presence of highly charged pentacarbonate species [31]. Using thermodynamic modelling, Kim et al. [8] reported ternary complexes such as $Th(OH)_3CO_3^-$, $Th(OH)_2(CO_3)_3^{4-}$, $Th(OH)(CO_3)_5^{5-}$, $Th(OH)_2CO_3$(aq), $Th(OH)_2(CO_3)_2^{2-}$, $Th(OH)_4(CO_3)^{2-}$, which are the most probable predominant aqueous Th(IV) species under many natural conditions [8].

At high pH close to pH 11.2, the higher concentration of OH^- ions has been found to enhance the formation of $Th(OH)_4$, and thus decrease the proportion of carbonate complexes in solution. Therefore, the measured solubility of Th(IV) in alkaline solutions is very close to the solubility in carbonate-free solutions [8].

590 **Table 2.** The initial dissolution rates [mol/g^{-1}s^{-1}] calculated for
591 samples A and E and their parallel samples B and F, according to
592 Equation (1).

Atmosphere and filtration	Solution	pH	Particle size	Test A (E) slope, dc/dt [molL-1day-1]	Test A (E) rate [mol g-1s-1]	Test B (F) slope, dc/dt [molL-1day-1]	Test B (F) rate [mol g-1s-1]	Data in Figure
Air (filtered)	0.01M NaCl (2mM $NaHCO_3$)	8	2-4mm	1.00E-13	**2.00E-19**			Fig 7B
Air (filtered)	0.1M NaCl	6	2-4mm	2.00E-14	**4.10E-20**			Fig 7A
Air	0.01M NaCl (2mM $NaHCO_3$)	8	2-4mm	5.00E-12	1.10E-17			Fig 7B
Air	0.1M NaCl	6	2-4mm	3.00E-13	6.10E-19			Fig 7A
Argon (filtered)	0.1M NaCl	6	80-160um	5.40E-11	**2.10E-16**	2.90E-11	**1.10E-16**	Fig 8b
Argon (filtered)	0.1M NaCl	5	2-4mm	2.90E-11	**1.00E-16**	8.40E-12	**2.10E-17**	Fig 8d
Argon (filtered)	0.01M HNO_3	2	80-160um	6.70E-09	**2.70E-14**	5.80E-09	**2.20E-14**	Fig 8f
Argon (filtered)	0.01M HNO_3	2	2-4mm	6.30E-09	**2.30E-14**	4.40E-09	**1.70E-14**	Fig 8h
Argon	0.1M NaCl	5	80-160um	4.20E-10	1.70E-15	1.50E-10	5.60E-16	Fig 8a
Argon	0.1M NaCl	4	2-4mm	4.40E-11	1.50E-16	9.20E-12	2.30E-17	Fig 8c
Argon	0.01M HNO_3	2	80-160um	3.10E-08	1.30E-13	9.30E-09	3.50E-14	Fig 8e
Argon	0.01M HNO_3	2	2-4mm	6.50E-09	2.40E-14	4.40E-09	1.70E-14	Fig 8g

593

Atmosphere and filtration	Solution	pH	Particle size	Test A (E) slope, dc/dt [molL-1day-1]	Test A (E) rate [mol g-1s-1]	Test B (F) slope, dc/dt [molL-1day-1]	Test B (F) rate [mol g-1s-1]
Air (filtered)	0.01M NaCl (2mM $NaHCO_3$)	8	2-4mm	1.0E-13	**2.0E-19**		
Air (filtered)	0.1M NaCl	6	2-4mm	2.0E-14	**4.1E-20**		
Air	0.01M NaCl (2mM $NaHCO_3$)	8	2-4mm	5.0E-12	1.1E-17		
Air	0.1M NaCl	6	2-4mm	3.0E-13	6.1E-19		
Argon (filtered)	0.1M NaCl	6	80-160µm	5.4E-11	**2.1E-16**	2.9E-11	**1.1E-16**
Argon (filtered)	0.1M NaCl	5	2-4mm	2.9E-11	**1.0E-16**	8.4E-12	**2.1E-17**
Argon (filtered)	0.01M HNO_3	2	80-160µm	6.7E-09	**2.7E-14**	5.8E-09	**2.2E-14**
Argon (filtered)	0.01M HNO_3	2	2-4mm	6.3E-09	**2.3E-14**	4.4E-09	**1.7E-14**
Argon	0.1M NaCl	5	80-160µm	4.2E-10	1.7E-15	1.5E-10	5.6E-16
Argon	0.1M NaCl	4	2-4mm	4.4E-11	1.5E-16	9.2E-12	2.3E-17
Argon	0.01M HNO_3	2	80-160µm	3.1E-08	1.3E-13	9.3E-09	3.5E-14
Argon	0.01M HNO_3	2	2-4mm	6.5E-09	2.4E-14	4.4E-09	1.7E-14

594 If reader is interested in calculating the dissolution rate to units
595 [mol m^{-2}s^{-2}], one can e.g divide the values by 3.3cm^2/g in cases of
596 2mm particle size and 80cm2/g in cases of 80µm.

597 **3.3.4 Solubility of ThO_2**
598
599 The solubility levels at the end of the experiments were
600 compared with the equilibrium data of ThO_2 and $Th(OH)_4$,
601 which were taken from the Thermochimie database
602 [NEA/TDB] (Fig. 9). It should be noted that, for example,
603 in the experiment with 2 to 4 mm particles in 0.1 M NaCl
604 under Ar, there was still some decrease in Th concentration
605 at the end of the 90 days experiment. Thus, the solubility
606 level had probably not been stabilized to a steady state
607 during the experiments. The solubilities measured at pH 2
608 were at a lower level than would be expected from the
609 thermodynamics. Similar observations have been made by

Neck et al. [11]. In their undersaturation dissolution experiments, conducted also with crystalline ThO_2 in acidic conditions, the solubilities stayed below the theoretical solubility of ThO_2. In their experiments they also showed that the value of the solubility product was dependent on the crystallite size. In this study, the solubility values at a pH range of 4 to 8 can be plotted between the theoretical solubilities of crystalline ThO_2 and amorphous $Th(OH)_4$ (Fig. 9). Compared to the studies discussed by Neck et al. 2003 and Vandenborre et al. 2010 [11, 6], the values presented here are at an even lower level. This could be an effect of the crystallinity and relatively high sintering temperature of the ThO_2 utilized in these studies, however the usage of a sector field ICP-MS enabled an extremely accurate analyses of dissolved Th concentrations (down to a concentration of 10^{-12} mol/L), which is lower than achievable with conventional quadrupole ICP-MS MS, used in most other studies of Th solubility.

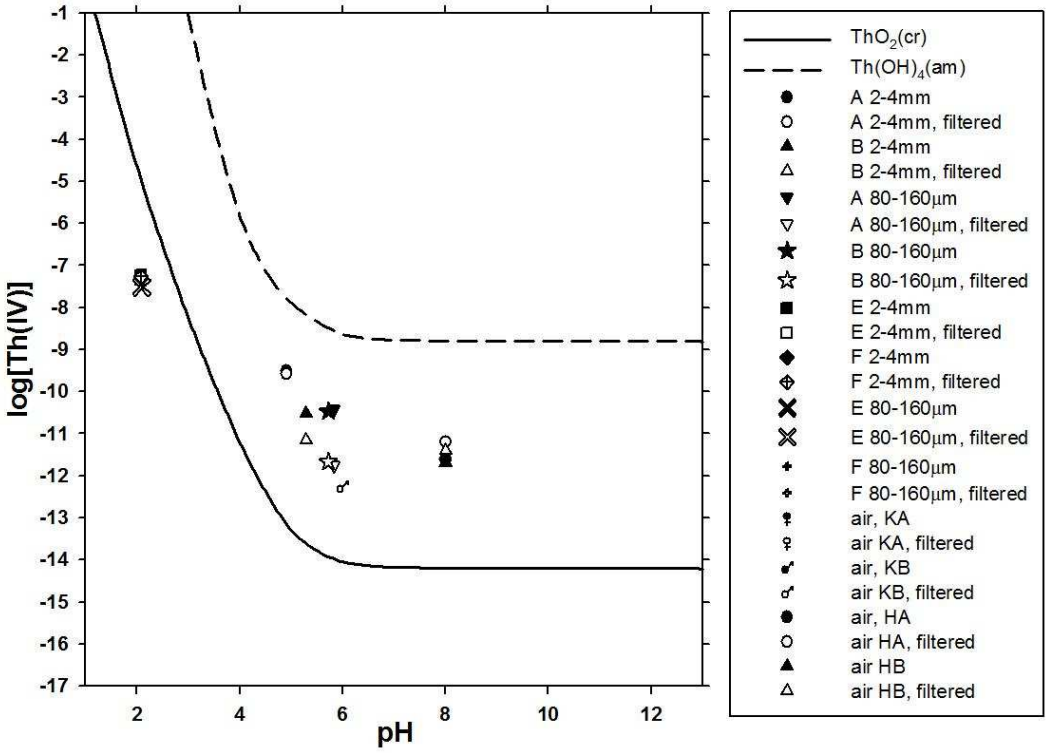

Fig. 9. The solubility levels of Th after ~100 days of dissolution in a suite of media investigated in the current work, compared to the Thermochimie equilibrium data for ThO_2 and $Th(OH)_4$ [NEA/TDB].

3.4 SEM imaging of leached ThO_2 surfaces

The SEM images of the HNO_3 leached ThO_2 particles revealed that the nature of the dissolution/precipitation phenomenon varied among the particles present in same solution. Some particles did not appear different from the fresh and unreacted particles (see Figures 10a and Figure 6, respectively). However, in a single particle, some surfaces

showed textures indicative of grain boundary dissolution (Figs. 10b – d), while others appeared to host a "blanket" of secondary phases precipitated from solution. In the former, grain rounding and widening of the grain boundaries was observed (Fig. 10b).

These results are in agreement with Corkhill et al. [29] who found that during dissolution in 0.01M HNO_3, grain boundaries of ThO_2 and CeO_2 analogues for UO_2 fuel dissolved rapidly, giving rise to enhanced initial dissolution rates. Furthermore, they found that surfaces with a grain boundary texture (like those shown in Fig. 10a) dissolved at much less rapid rate than surfaces with no grain boundaries, such as those that would be found on the surface of a sintered pellet. This may be the cause of the different particle morphologies described in the current investigation.

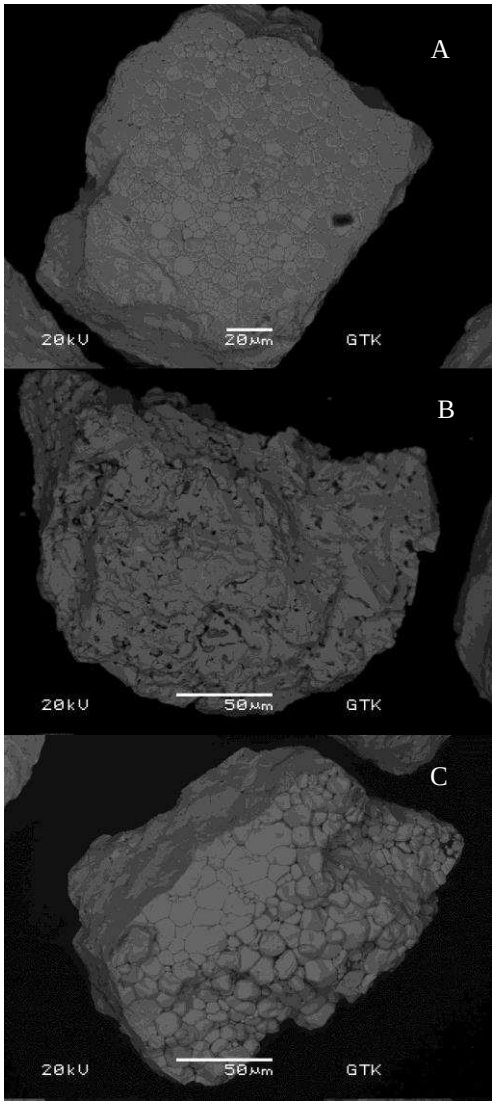

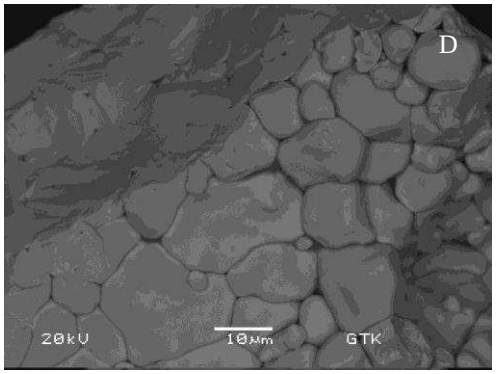

Fig. 10. BSE images of 80 to 160 µm ThO_2 particle after 4 weeks of leaching with 1 M HNO_3 at 80°C. A) a leached particle resembling a fresh one, B) a particle showing deeper dissolution, which has deformed the grain boundaries and formed some cavities into the ThO_2 particle. C and D are taken from this particle, which showed both areas of dissolution and no reaction.

4. Conclusions

ThO_2 pellets were synthesised to resemble the microstructure of the UO_2 matrix of nuclear fuel pellets. The pellets sintered at 1750 ° C had randomly oriented crystals and a grain size ranging from 10 to 30 µm.

Dissolution experiments were performed to study the effect of carbonate complexation on these ThO_2 samples. It was observed that the solubility and dissolution of ThO_2 increased in the presence of carbonate. The solubilities and dissolution rates of ThO_2 were also dependent on the H^+ activity of the solution. The acidic conditions were found to increase the solubility compared to near-neutral and basic conditions, in which sparingly soluble hydrolysed species of Th were the dissolution-controlling factor. In these experiments the concentration of Th ($\geq 10^{-9}$ mol/L) at pH ≤ 4 was slighly lower than the theoretical solubility of crystalline ThO_2. HR-ICP-MS, with magnetic sector field capability, allowed the analyses of dissolved Th concentrations of sparingly soluble ThO_2 phases down to 10^{-12} mol/L. At higher pH values, from pH 4 to pH 8, the measured concentrations (10^{-10} to 10^{-12} mol/L) were between the theoretical solubility of ThO_2 and $Th(OH)_4$.

Particle size was also found to have an effect on the solubility. The smaller particles with greater surface area seem to have enhancing effect on initial dissolution, and sorption/precipitation reactions. In agreement with recent results [29], it is hypothesized that high energy surface sites may play a role in the relatively rapid initial release of Th observed here. The results of the surface analyses indicated that the initial surface condition may also have some effect on the dissolution processes, with grain boundaries likely playing an important role.

Acknowledgements. This study has been a part of REDUPP project. The research leading to these results has received funding from the European Atomic Energy Community's Seventh Framework Programme (FP7) under grant agreement No. 269903. The high voltage pulse power fragmentation method, Selfrag fragmentation, of the ThO_2 pellets and SEM imaging of the leached parti-

cles were carried out at the Finnish Geological Survey (GTK). We thank Jukka Marmo and Marja Lehtonen from GTK for their work and expertise. We thank also Jaana Rantanen and Merja Tanhua-Tyrkkö from VTT. They took part to the Th analyses and data treatment, respectively. We are grateful to Dr.Virginia Oversby and Dr. Lena Z. Evins for invaluable discussion and support throughout the project. We thank Posiva, SKB, VTT for their financial support. CLC acknowledges The University of Sheffield for the award of a Vice Chancellor's fellowship NCH is grateful to the Royal Academy of Engineering and Nuclear Decommissioning Authority for financial support.

References

1. Morss, L.R., Edelstein, N.M., Fuger, J. & Katz, J.J.,The chemistry of the actinide and transactinide elements. Springer 2006.

2. Dekoussar, V., Dyck, G.R., Galperin, A., Ganguly, C., Todosow, M. & Yamawaki, M. Thorium fuel cycle – Potential benefits and challenges. IAEA, IAEA-TECDOC-1450, Vienna, 2005

3. Alexander, W.R., and McKinley L.E. (ed.) Deep geological Disposal of Radioactive Waste, Elsevier Series Radioactivity in the Environment, Vol 9. 2008

4. Combie, C., Pescatore, C., Smith, P. and van Luik, A., Geological Disposal of Radioactive Waste; Review of Developments in the Last Decade, OECD Publications, 2, rue Andr´e-Pascal, 75775 PARIS CEDEX 16, France
(66 1999 17 1 P) ISBN 92-64-17194-0 – No. 51101 1999

5. Vandenborre, J., Abdelouas A., Grambow, B., Discrepancies in Thorium Oxide Solubility Values: a new experimental approach to improve understanding of oxide surface solid/solution. RadioChim Acta **96**, 515-520.(2008)

6. Vandenborre, J., Grambow, B. & Abdelouas, A., Discrepancies in Thorium Oxide Solubility Values: Study of Attachment/Detachment Processes at the Solid/Solution Interface. Inorganic chemistry. **49**, No. 19, 8736-8748 (2010)

7. Neck, V. & Kim, J., Solubility and hydrolysis of tetravalent actinides. Radiochim. Acta, **89**, No. 1/2001, 1, (2001)

8. Kim, S., Baik, M., Choi, J., Shin, H. & Yun, J., The dissolution of ThO 2 (cr) in carbonate solutions and a granitic groundwater. Journal of Radioanalytical and Nuclear Chemistry, **286**, No. 1, pp. 91-97 (2010)

9. Fuger, J., Rand, M., Grenthe, I, Neck, V., & Rai, D. Chemical Thermodynamics of Thorium, OECD Nuclear Energy Agency. (2007)

10. Neck, V., Müller, R., Bouby, M., Altmaier, M., Rothe, J., Denecke M.A. & Kim, J.I., Solubility of amorphous Th(IV) hydroxide – application of LIBD to determine the solubility product and EXAFS for aqueous speciation. Radiochim. Acta, **90**, pp. 485. (2002)

11. Neck, V., Altmaier, M., Müller, R, Bauer, A, Fanghänel, Th, and KIM J.I. Solubility if crystalline thorium dioxide, Radiochim. Acta **91**, 253-262, (2003)

12. Schindler, P.W., Heterogenous equilibria involving oxides, hydroxides,carbonates and hydroxide carbonates. Adv. Chem. Ser. **67**,196 (1967)

13. Bundschuh, T., Knopp, R., Müller, R., Kim, J., Neck, V. & Fanghänel, T., Application of LIBD to the determination of the solubility product of thorium (IV)-colloids. Radiochim. Acta, **88**, No. 9-11/2000, pp. 625. (2000)

14. Rothe, J., Denecke, M., Neck, V., Müller, R. & Kim, J., XAFS investigation of the structure of aqueous thorium (IV) species, colloids, and solid thorium (IV) oxide/hydroxide. Inorganic chemistry, **41**, No. 2, pp. 249-258 (2002)

15. Bitea, C., Müller, R., Neck, V., Walther, C. & Kim, J., Study of the generation and stability of thorium (IV) colloids by LIBD combined with ultrafiltration. Colloids and Surfaces A: Physicochemical and Engineering Aspects, **217**, No. 1, pp. 63-70. (2003)

16. Altmaier, M., Neck, V. & Fanghänel, T., Solubility and colloid formation of Th (IV) in concentrated NaCl and MgCl2 solution. Radiochimica Acta/International journal for chemical aspects of nuclear science and technology, **92**, No. 9-11/2004, pp. 537-543. (2004)

17. Walther, C., Fuss, M. & Buchner, S., Formation and hydrolysis of polynuclear Th (IV) complexes-a nano-electrospray mass-spectrometry study. Radiochim. Acta, **96**, No. 7, pp. 411-426, (2008)

18. Hubert, S., Barthelet, K., Fourest, B., Lagarde, G., Dacheux, N. & Baglan, N.. Influence of the precursor and the calcination temperature on the dissolution of thorium dioxide. Journal of Nuclear Materials, **297**, No. 2, pp. 206-213, (2001)

19. Forsyth R., Fuel rod D07/B15 from Ringhals 2 PWR: Source material for corrosion / leach tests in groundwater. Fuel rod / pellet characterisation program part 1. SKB technical report 87-02. (1987)

20. Forsyth R., Spent nuclear fuel. A review of properties of possible relevance to corrosion processes. SKB technical report 95-23. (1995)

21. Stennett, M. C. Corkhill, C.L, Marshall, L. A. Hyatt, N.C., J. Nucl.Mater., **432**, 182 (2013)

22. Andres, U., Timoshkin, I. and Jirestig, J., Liberation of minerals by high-voltage electrical pulses. Powder Technology, 104, 37-49. (1999)

23. Bluhm H., Frey W., Giese H., Hoppe P., Schultheiβ C., Straβner R., Application of Pulsed HV Discharges to Material Fragmentation and Recycling, IEEE Trans. On Dielectrics and Electrical Insulation, 7, No.5, (2000)

24. Rozalén M. L., Huertas F. J., Brady P. V, Cama J., García-Palma S., Linares J., Experimental study of the effect of pH on the kinetics of montmorillonite dissolution at 25˚C, Geochimica et Cosmochimica Acta, **72**(17), 4224-4253, (2008)

25. Malmström M., Banwart S., Lewenhagen J., Duro L., Bruno J., The dissolution of biotite and chlorite at 25˚C in the near-neutral pH region, Journal of Contaminant Hydrology, **21**(1-4), 201-213, (1996)

26. Brady P., Walther J.V., Kinetics of quartz dissolution at low temperatures, Chemical Geology, **82**, 253-264, (1990)

27. Brantley, S.L., Kinetics of mineral dissolution

Brantley, S.L., Kubicki, J.D., White, A.F., (Eds.), Kinetics of Water–Rock Interaction, Springer-Kluwer, New York (2008)

28. Weast R.C. (ed), CRC Handbook of Chemistry and Physics, 53rd Edition, The Chemical Rubber Co. Cleveland, Ohio, USA, (1972)

29. Corkhill, C.; Myllykylä, E.; Bailey, D.; Thornber, S.; Qi, J.; Maldonado, P.; Stennett, M.; Hamilton, A.; Hyatt, N. The contribution of energetically reactive surface features to the dissolution of CeO_2 and ThO_2 analogues for spent nuclear fuel, submitted to ACS Applied Materials & Interfaces. Manuscript ID: am-2014-018978.

30. Zetterström Evins, L. & Vähänen, M.(eds.), REDUPP First Annual Report, Posiva Oy, Olkiluoto, Finland, Posiva Working Report 2012-28, 44 p (2012)

31. Rai, D., Felmy, A.R., Moore. D.A., & Mason, M.J., 1995. The solubility of Th(IV) and U(IV) hydrous oxides in concentrated $NaHCO_3$ and Na_2CO_3 solutions. (1995)" In Scientific Basis for Nuclear Waste Management XVIII, Part 2, T. Murakami and R. C. Ewing (eds.), pp. 1143-1150, Materials Research Society Symposium Proceedings, Volume 353, Materials Research Society, Pittsburgh, Pennsylvania.

32. Ötshols, E., Bruno, J. & Grenthe, I., 1994. The solubility of microcrystalline ThO_2 in CO-H_2O media, Geochim. et Cosmochim, Acta. 58, No. 2, pp. 613-623 (1994)

* Correspondence author (e-mail:emmi.myllykyla@vtt.fi)